Nanoscale

PAPER

View Article Online
View Journal | View Issue

Cite this: *Nanoscale*, 2025, **17**, 12704

Gel polymer electrolytes for room-temperature sodium sulfur batteries†

Hao Nguyen, Jiahan Li, Raju Vadthya and Shuya Wei*

Sodium sulfur batteries have gained attention owing to their advantages of low cost and high specific capacity. However, the current electrolytes have a few main disadvantages including sodium-dendrite growth, sulfur shuttling and electrolyte leakage, which hinder their practical application. Herein, we report the preparation of poly(vinylidene fluoride-*co*-hexafluoropropylene)-based gel polymer electrolytes using a simple solution casting technique for room-temperature sodium sulfur battery applications. The gel polymer electrolyte was activated by soaking the freshly prepared gel polymer membranes in a liquid electrolyte solution. Our gel polymer electrolyte exhibited a high ionic conductivity of 1.37 mS cm^{-1} at ambient temperature, with an electrochemical stability window of 4.5 V *versus* Na^+/Na. Furthermore, sodium symmetric cells showed stable stripping/plating of Na^+ up to 3000 hours, with a transference number of 0.648. The cells achieved a specific capacity of 398 mA h g^{-1} for the initial reversible discharge specific capacity and 75 mA h g^{-1} at cycle 200 with 99.9% coulombic efficiency at 0.1 C rate. Our results demonstrate that these polymer electrolytes are potential candidates for sodium sulfur batteries with desired performance.

Received 11th March 2025,
Accepted 1st April 2025

DOI: 10.1039/d5nr01049g

rsc.li/nanoscale

1. Introduction

Nowadays, lithium-ion batteries are widely used for daily life activities in energy storage devices ranging from small portable electronic devices to medium electric vehicles and large power grid.[1,2] However, lithium is scarce, and its cost is rising due to the ongoing surge in demand for this battery technology. In view of that, developing materials that offer high energy density, greater abundance, and lower production costs is of utmost importance. Therefore, sodium–sulfur batteries (NaSBs), which use inexpensive and environmentally benign materials of sodium and sulfur, have attracted substantial interest in recent years due to their high specific capacity (1675 mA h g_{sulfur}^{-1}). Analogous to the components of a lithium-ion battery cell, a NaSB also comprises a cathode, an anode, a separator and an electrolyte. The major drawback of this conventional cell's configuration is the lack of safety due to flammable organic electrolytes in the system. Despite having high ionic conductivities (10^{-3} to 10^{-2} S cm^{-1}), conventional organic liquid electrolytes (LEs) present several significant issues. LEs can cause dendrite growth due to nonuniform current distribution. The main concern of using LEs arises from the risk of leakage leading to fire hazards.[3–5] Moreover, LEs suffer from significant disadvantages due to polysulfide shuttling effects. Compared to LEs, polymer electrolytes (PEs) are profoundly favored for energy storage applications since they can accommodate the volume changes of the electrodes amid electrochemical processes and encourage the adaptable

Department of Chemical and Biological Engineering, University of New Mexico, Albuquerque, New Mexico, USA. E-mail: swei@unm.edu

†Electronic supplementary information (ESI) available. See DOI: https://doi.org/10.1039/d5nr01049g

Shuya Wei

Dr Shuya Wei is an assistant professor in Chemical & Biological Engineering at the University of New Mexico. She earned her Ph. D. in Chemical Engineering from Cornell in 2017 and a B.Eng. from Nanyang Technological University in 2013. She was a postdoctoral fellow at MIT from 2017 to 2019. Dr Wei received the ORAU Ralph E. Powe Award, ACS Petroleum Research Fund DNI Award, and New Mexico Women in Technology Award. Her research focuses on electrochemical processes at electrodes and interfaces, aiming to develop high-energy-density metal-based batteries for energy and environmental applications.

designs of batteries with diverse shapes. Furthermore, the hindering effects such as leakage of electrolyte can be minimized by using polymer electrolytes.[6–9] However, solid polymer electrolytes also have some drawbacks such as low electrical conductivity (10^{-8} to 10^{-5} S cm^{-1}) at room temperature and poor electrode/electrolyte interfaces.[10–13] Various approaches have been explored to develop PEs that exhibit enhanced conductivity at room temperature and maintain stable interfaces between electrodes and electrolytes. Researchers have focused on improving the ionic conductivity of PEs under ambient conditions while ensuring robust interfacial properties to enhance the overall battery performance.[14–17]

With the aim to overcome the above-mentioned issues, the liquid electrolytes were incorporated into a solid polymer membrane to form gel polymer electrolytes (GPEs), which embraces both the characteristics of PEs and LEs.[14] The properties of the polymer membrane, essentially porosity, wettability, and tortuosity of the pores, are greatly influenced by its processing methods that involve distinctive techniques such as solution casting, phase inversion, UV curing, *in situ* polymerization and electrospinning method.[16,18–23] Among the available methods, solution casting stands out as the most straightforward yet modestly scalable approach. This technique involves blending the LEs with the polymer precursor, spreading the mixture onto a glass surface and then allowing it to dry in a vacuum chamber. Once the gel polymer electrolyte (GPE) membrane is freshly prepared, it is immersed in the same liquid electrolyte to absorb the solution and swell.

In GPEs, polyvinylidene fluoride (PVDF), poly vinylidene fluoride-*co*-hexafluoropropylene (PVDF-HFP), polyacrylonitrile (PAN), and polymethyl methacrylate (PMMA) have been widely used as polymer hosts. Among them, PVDF-HFP has received great attention because of their amorphous nature and its potentiality to display high room-temperature ionic conductivity, strong chemical resistance, high thermal stability and flexibility.[24–26] Moreover, PVDF-HFP-based GPEs have a high dielectric constant of 8.4 and a strong electron-withdrawing functional group (–C–F), which advances to the greater disintegration of salts and subsequently supports a high concentration of charge carriers.[27] Kumar *et al.*[9] successfully fabricated GPE using a PVDF-HFP backbone and SiO_2 as an additive for NaSBs. Despite having a high conductivity of 4.1 mS cm^{-1} and a sodium ion transport number of 0.52, the batteries failed to run multiple cycles and only produced a specific capacity of 165 mA h g^{-1} on the first discharge. Janakiraman *et al.*[25] reported the preparation of PVDF-HFP using a simple electrospinning technique and the GPE was activated by soaking in LE. The GPE has higher an ionic conductivity of 1.13×10^{-3} S cm^{-1} than commercial separator Celgard 2400 with 0.36×10^{-4} S cm^{-1}. However, there are many drawbacks in using the electrospinning technique, such as low commercial impact and scalability for large-scale applications due to limited production rate and another problem is its mechanical strength limitation, which could be a concern for energy storage where structural integrity is required.[28] The PVDF-HFP copolymer has received great attention as a polymer host GPE.[29,30] However, there are very few reports on PVDF-HFP as a polymer host synthesized by a solution casting technique for room-temperature NaSB applications. In particular, there is no report on how different compositions of organic electrolytes affect the conductivity and the performance of room-temperature sodium-sulfur batteries.

In the present work, we prepared a PVDF-HFP-based GPE by a solution casting technique. The ionic conductivities with different compositions of organic electrolytes were investigated. The GPE consists of 1 M sodium perchlorate ($NaClO_4$) in propylene carbonate (PC): ethylene carbonate (EC) (4 : 1 volume ratio), which showed the highest ionic conductivity of 1.37 mS cm^{-1} with a wide potential operation stability window of 4.5 V *vs.* Na^+/Na. Electrochemical characterization tests including cyclic voltammetry and galvanic charge–discharge cycles were conducted using assembled full cells. Notably, symmetric sodium cells underwent a stripping and plating test that continued uninterrupted for 3000 hours. This impressive performance indicates significant proficiency for developing sustainable sodium-sulfur batteries that offer high energy density and enhanced safety features.

2. Experimental section

2.1 Materials

Sodium cube (Na, 99.9%, Sigma-Aldrich), sodium perchlorate ($NaClO_4$, >98.0%, Sigma-Aldrich), propylene carbonate (PC, >99%, Sigma-Aldrich), ethylene carbonate (EC, 98%, Sigma-Aldrich), polyvinylidene fluoride-*co*-hexafluoropropylene (PVDF-HFP, average M_W 400 000, pellets, Sigma-Aldrich), and *N*-methyl-2-pyrrolidone (NMP, 99.9%, MSE Supplies) were stored in an Ar-filled glovebox (Vacuum Technology Inc., O_2 and H_2O < 0.01 ppm).

2.2 Material synthesis

2.2.1 Preparation for GPE membrane. The LEs were prepared by dissolving 1 M $NaClO_4$ in PC : EC (x/1 volume ratio, where x = 1 and 4) and 1 M $NaClO_4$ in PC under stirring overnight and the obtained LEs will be denoted as LE11, LE41 and LEPC. First, gel polymer precursors were prepared by dissolving poly(vinylidene fluoride-*co*-hexafluoropropylene) (PVDF-HFP, average M_W 534 000, powder, Sigma-Aldrich) in NMP with 1 : 4 weight ratio overnight. Then, the gel polymer precursors will be stirred with different LEs at 1 : 1 weight ratio at 50 °C overnight and will become GPE precursors. After that, GPE precursors were cast at 80 μm thickness on a 50 °C preheated glass plate using doctor blade and will be dried at 50 °C for 12 hours under vacuum environment. The dried GPE was cut into $\frac{3}{4}$ inch diameter and soaked in the same composition of its LE overnight and will be denoted as GPE11, GPE41 and GPEPC. For example, 0.4 g of PVDF-HFP and 1.6 g NMP were mixed overnight. Then, 2 g of LE11 was added and stirred overnight. After casting, vacuum drying and cutting, the GPE membrane will be immersed in LE11 overnight and become GPE11.

2.2.2 Preparation of sulfur/polyacrylonitrile (SPAN) cathodes. SPAN was synthesized following Wei *et al.* experiment.[31] In brief, sulfur (*S*, 99.998%, Sigma-Aldrich) was mixed with polyacrylonitrile (PAN, average M_W 150 000 (typical), Sigma-Aldrich) with 4 : 1 weight ratio using a ball mill machine for 4 hours. The SPAN powder was placed in a tube furnace and heated at 450 °C at 5 °C min^{-1} ramping rate in an Ar flow environment for 6 hours. The baked SPAN was mixed with carbon black (super P, MSE) and 5 wt% PVDF in NMP mixture with a weight ratio of 8 : 1 : 1, respectively, with additional NMP to lessen the viscosity. Next, the prepared compound was mixed by using a vortex mixer and a sonication bath. The as-prepared slurry was cast onto carbon-coated aluminum foil (16 μm, MTI Co., USA) with a thickness of 20 μm using doctor blade. The coating was dried overnight at 70 °C in a vacuum oven. Finally, cathodes with 12.7 mm diameter were punched out and stored in the glovebox. The obtained cathodes have an average sulfur loading of 0.79–1.26 mg cm^{-2}.

3. Characterization

3.1 Physicochemical characterization

Functional group identification and probable inter/intra-molecular interactions were characterized by Fourier transform infrared (FTIR) spectroscopy (The Nicolet 6700 FTIR Spectrometer), in the range of ~4000–400 cm^{-1} by averaging 64 scans with a resolution of ~2 cm^{-1}. Scanning electron microscopy (SEM) was employed (TESCAN VEGA with an accelerating voltage of 2.0 kV) on the dried and soaked GPE41 samples to evaluate the morphology. Thermogravimetric analysis (TGA) was performed using a TGA 5500 in the temperature range from room temperature to 800 °C with 5 °C min^{-1} in a N_2 environment. Differential scanning calorimeter (DSC) data were acquired using a Netzsch STA 449 F3 Jupiter TGA/DSC instrument. The sample with ~10–20 mg was cooled to −100 °C from its initial temperature and then it was heated from −100 °C to 100 °C at 5 °C min^{-1} rate under a N_2 atmosphere.

3.2 Electrochemical characterization

Electrochemical tests were performed in R2032 cells assembled in an Ar-filled glovebox (O_2, H_2O < 0.01 ppm). Fresh Na metal cube was cut, pressed and punched into 12.7 mm diameter electrode with a thickness of ~0.2 mm. A full cell consists of a Na metal anode, a GPE and a SPAN cathode. For LE cells, Whatman™ GF/A separators were used and punched into $\frac{3}{4}$ inch diameter with 80 μL electrolyte of 1 M $NaClO_4$ in PC. Cell fabrication was carried out in an argon-filled glovebox and rested for 12 hours before electrochemical characterization. For linear sweep voltammetry (LSV) study, a cell with stainless steel as the working electrode and sodium metal as the counter electrode/reference electrode will be examined at a scan rate of 0.1 mV s^{-1} along the voltage window between −0.2 and 5 V *vs.* Na/Na^+. Potentiostatic electrochemical impedance spectroscopy (PEIS) were performed using a Biologic SP-50e integrated frequency response analyzer. PEIS was performed at a constant voltage of 10 mV alternating current with frequencies ranging from 800 kHz to 100 mHz. Cyclic voltammetry (CV) measurements were performed between 0.8 and 3 V, using SPAN as the working electrode and sodium as the reference and counter electrodes with different scan rates using Biologic MPG-2. Galvanostatic charge/discharge (GCD) and a stripping/plating test was performed using a NEWARE battery testing system. Galvanostatic cycling was performed at different C rates (1C = 1675 mA h g_s^{-1}) with the voltage window between 0.8 and 3 V *vs.* Na/Na^+.

4. Results and discussion

The morphology evolution of GPE was systematically investigated using SEM shown in Fig. 1(a–c) and Fig. S5. In the dried state (Fig. 1a and S5a†), the GPE membrane exhibited a porous surface morphology with pores diameter of 1–5 μm. This interconnected porous structure facilitates efficient absorption of liquid electrolyte while mitigating leakage risks.[9] Moreover, this porous framework provides sufficient space for the expansion of polymer matrix after LE absorption. Following overnight soaking in LE, PVDF-HFP matrix underwent significant swelling (Fig. 1b and S5b†), encapsulating the electrolyte within its structure. The expansion of the membrane potentially enhances internal surface contract between polymer chains, thereby promoting ion transport pathways and elevating ionic conductivity. Additionally, the interfacial contact area between the electrode and the electrolyte also increases with swollen GPE, which is critical for electrochemical performance. Cross-sectional SEM image (Fig. 1c) revealed a uniform membrane thickness of ~120 μm and the GPE membrane is thinner than the commercialized Whatman™ GF/A separator (260–290 μm). Crucially, the polymer matrix retained structural consistency after both vacuum drying and LE immersion, demonstrating robust mechanical stability and no observable degradation of the PVDF-HFP framework.

FTIR spectroscopy studies (Fig. 1d) were performed to examine the molecular interactions between the liquid electrolyte and the polymer matrix, as well as to analyze the changes in the polymer host due to the entrapment and dispersion of the $NaClO_4$-containing liquid electrolyte. Fig. 1d illustrates the comparative FTIR spectra of pristine PVDF-HFP, LE41, dried GPE41, and soaked GPE41, within the wavenumber range of 400 to 2000 cm^{-1}. The assignment of the important IR bands associated with the host polymer PVDF-HFP, PC, EC, and perchlorate (ClO_4^-) anions is given in the ESI (Table S1†).

The following distinctive features have been extracted from the spectral response: the peaks at 877 and 842 cm^{-1} present α phase conformation of the semi-crystalline PVDF-HFP.[32–36] The α phase peaks slightly shift to a higher wave number after incorporating LE into a polymer matrix.[9] The peaks at 1675 cm^{-1} represent the C═O stretching vibration of the NMP solvent entrapped in the GPE. The peaks at 1397 cm^{-1} and 1187 cm^{-1} show C–H_2 and C–F_3 stretching in PVDF-HFP,

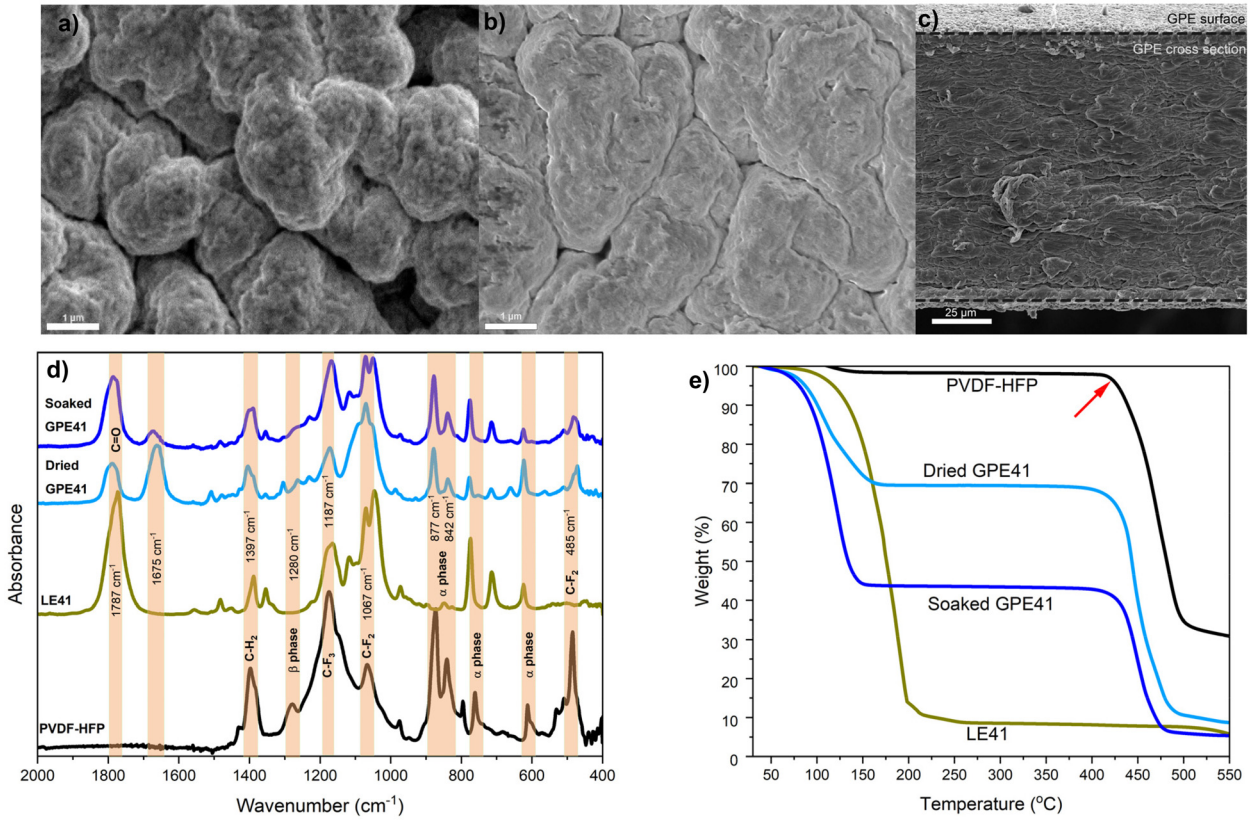

Fig. 1 SEM image of (a) dried GPE41 and (b) soaked GPE41. (c) SEM image of the cross-section of soaked GPE41. (d) FTIR spectra of pristine PVDF-HFP, LE41, and GPE41 after vacuum-drying and GPE41 after soaking in LE41. (e) TGA of pristine PVDF-HFP, dried GPE41, soaked GPE41 and LE41.

respectively.[37–39] The peak at 1787 cm^{-1} corresponds to cyclic carbonate in PC and EC, which shifts to a higher position of 1807 cm^{-1} in both dried and soaked GPEs. This behavior corresponds to the H–C═C–F stretching vibration modes of polyene, suggesting the partial dehydrofluorination of PVDF-HFP chains.[40] The NMP solvent functions as a Lewis base, which induces chemical dehydrofluorination of the PVDF-HFP skeleton to activate the movements of PVDF-HFP chains, which enhances the interactions among polymer chains.[41] The dehydrofluorination process can enhance the amorphous content of the polymer, potentially resulting in higher LE absorption and improved ionic conductivity of the electrolyte.[42] These observations indicate a complex interplay between the solvent, polymer and electrolyte components, leading to structural modifications that may significantly influence the GPE's electrochemistry properties.

To further examine the material's thermal behavior, thermal gravimetric analysis was used. Fig. 1e shows the thermal gravimetric curves from the PVDF-HFP membrane, LE11, dried GPE41 and soaked GPE41. The PVDF-HFP membrane shows thermal stability until 140 °C and its initial mass reduction around 170 °C is related to the evaporation of NMP components. No weight loss has been observed for PVDF-HFP after 140 °C until reaching 420 °C, where PVDF-HFP decomposition happens. A gradual weight loss of ~5 wt% around 100 °C for dried GPE41 and soaked GPE41 samples is possibly attributed to the loss of moisture absorbed by the polymer from the experimental environment. The substantial weight loss that occurred between 120 °C and 200 °C was due to the evaporation of LE in dried GPE41 and soaked GPE41. This weight loss reveals that more than 20 wt% of LE41 was incorporated inside the dried GPE41 after the synthesis process. Along with immersing the dried membrane GPE41 into LE41 overnight, GPE41 swelled and became transparent (showed in Fig. S1†) increasing the LE content to more than 50 wt%. The polymer PVDF-HFP and GPE underwent a second significant mass reduction between 450 °C and 500 °C, matching with the beginning of its thermal decomposition. During this stage, the PVDF-HFP structure begins to break down thermally, and the backbone of the polymer starts to degrade.[43–45] This stage marks a critical point (indicated by the red arrow in Fig. 1e) in the material's thermal behavior and represents polymer molecular structure deterioration due to the high temperatures.

The electrochemical stability window or potential window represents a voltage range within which an electrolyte can remain stable without undergoing unwanted side reactions. This crucial parameter plays a significant role in determining the maximum operating voltage of a battery, directly influen-

cing its energy density and longevity. A wider electrochemical stability window allows for higher operating voltages, potentially enhancing the battery performance. LSV measurements of GPEs in Fig. 2a illustrates the electrochemical stability windows of GPEPC, GPE11, and GPE41. The graph shows a pair of redox peaks at around 0 V, which correspond to the sodium ion plating and stripping on electrodes.[46] The cell ran steadily with no change in current up to 4.5 V (*vs.* Na^+/Na) at ambient temperature, which indicates that the GPE does not have any impurity during the fabrication process, and it did not undergo any side reaction with sodium metal. The degradation of the GPE membrane occurs beyond 4.5 V, which is more than sufficient to operate NaSBs at room temperature. Typically, an GPE that does not undergo a redox reaction under the battery working voltage range (0.8 to 3 V in this work) can be considered as an ideal GPE.[47–49] The wide electro-

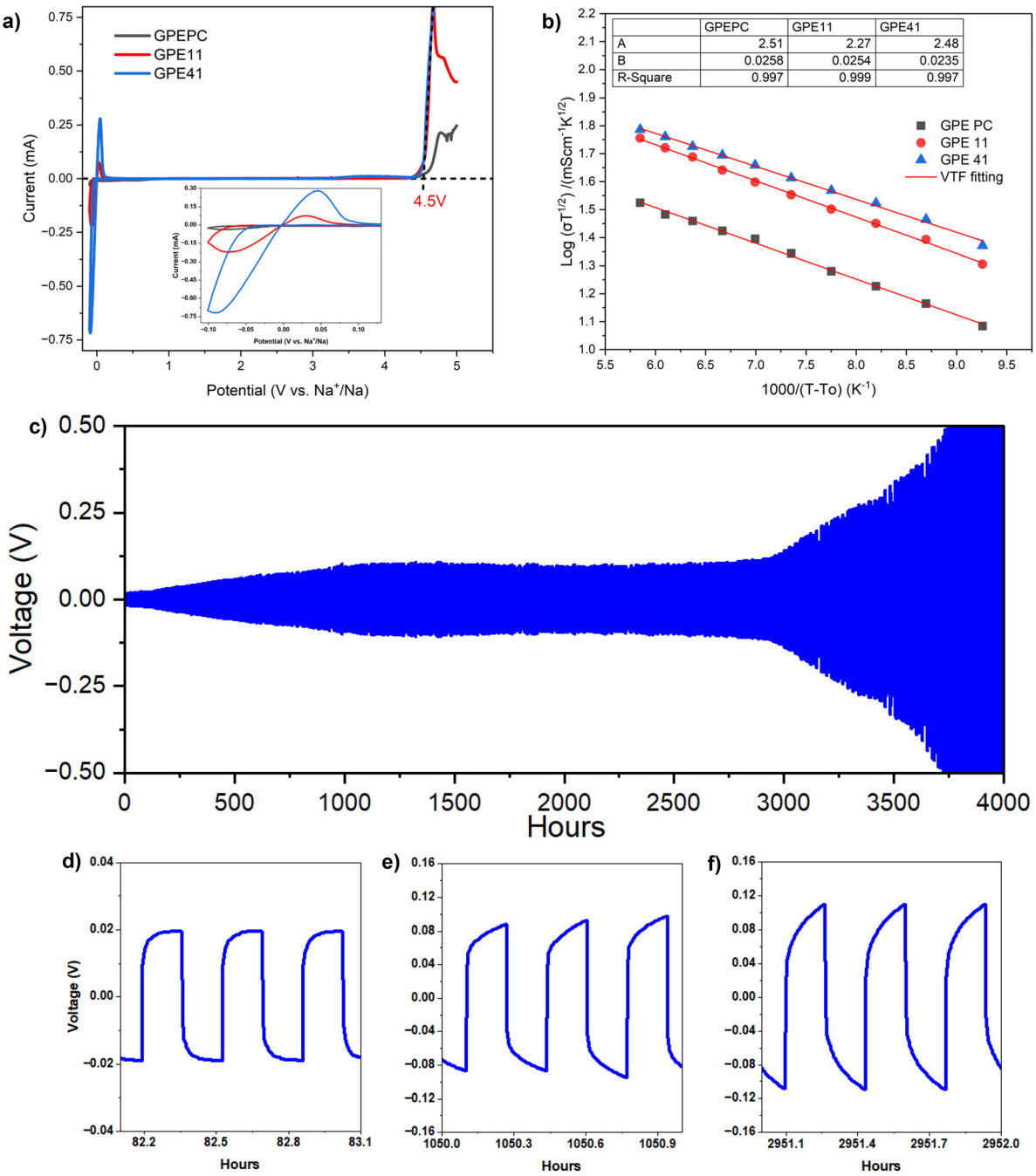

Fig. 2 (a) LSV of GPE containing various compositions in the voltage range of −0.10 V to 5 V at a scan rate of 0.1 mV s^{-1}. (b) VTF fitted plots of ionic conductivity for polymer electrolytes containing various compositions. The inset table in Fig. 2b summarizes the VTF parameters of B determined from the linear plot $\log \sigma T^{1/2}$ *versus* $1/(T - T_o)$. (c) Galvanostatic stripping and plating performance of symmetric cells Na|GPE41|Na and (d–f) zoomed-in view at different times.

chemical window (0–4.5 V) plays an exceedingly important role in the electrochemical stability of NaSBs. As the new energy density and voltage of the new generation of batteries increases, the separator film also faces challenges of bearing a high voltage. This wide range of electrochemical potential is more than sufficient to operate not only for NaSBs but also for sodium ion batteries, which makes GPE41 as an ideal electrolyte candidate for both NaSBs and sodium ion batteries.[7,50–53]

Table S2† shows the ionic conductivities of GPE PC, GPE 11 and GPE41 at various temperatures using AC impedance spectroscopy and conductivity eqn (1):

$$\sigma = \frac{L}{AR_b} \quad (1)$$

where L is the thickness of the membrane, A is the area of the membrane, and R_b is the bulk resistance from the EIS plot.

The GPE membrane was placed between stainless steel surfaces to fabricate SS|GPE|SS coin cells for conductivity measurement. Fig. 2b shows the temperature variations of the conductivity of all the polymer complexes. As the temperature increases, the conductivity also increases for all the compositions. The non-linearity in Arrhenius plots indicates that ion transport in polymer electrolytes is dependent on polymer segmental motion. The curvature behavior of the plots suggests that the data can be better described by the Vogel–Tamman–Fulcher (VTF) equation, typical of disordered systems:[54]

$$\sigma = AT^{-1/2} \exp\left(\frac{-B}{k_B(T - T_o)}\right) \quad (2)$$

where A is a fitting constant proportional to the number of charge carriers, B the pseudo-activation energy associated with the motion of the polymer segment, k_B the Boltzmann constant and T_o is taken as the equilibrium temperature of the system corresponding to zero configuration entropy. T_o was found to be equal to $T_g - 50$ K, where T_g represents the thermodynamic glass transition temperature of the samples (Fig. S6†).[55–57] As shown in Fig. 2b, the VTF plot was well fitted for all studied GPE ($R^2 > 0.99$). GPE41 had the lowest pseudo-activation energy at 0.0235 eV and the highest conductivity at 1.37 mS cm^{-1} at ambient temperature, compared to 0.0254 eV with 1.17 mS cm^{-1} and 0.0258 eV with 0.7 mS cm^{-1} for GPE11 and GPEPC, correspondingly. As the temperature rises, polymer chains in electrolytes experience more rapid bond rotations and enhanced segmental motion. This enhanced molecular mobility creates a more favorable environment for ion transport, facilitating both inter-chain hopping and intra-chain movement of ions.[58] The combined effect improved ion transport mechanisms results in an increase in the overall ionic conductivity of the polymer electrolyte. This temperature-dependent behavior is crucial for understanding and optimizing the performance of polymer electrolytes in various applications. The increased sodium ion mobility leads to improved overall ionic conductivity in the electrolyte. More efficient ion transport can lead to more uniform plating and stripping of sodium at the electrode surfaces, potentially reducing dendrite formation and improving long-term cycling stability.[59,60] To gain insights into the plating and stripping behavior of Na, the galvanostatic cycling test was employed in symmetric Na|GPE41|Na coin cells. The coin cell was applied 0.1 mA cm^{-2} for 15 minutes of charge and 15 minutes of discharge. The plating and stripping test in Fig. 2c shows the utilized GPE41 symmetric cell can run over thousands of cycles and approach 3000 hours of operation before the overpotential significantly increased due to long operation and possibly electrolyte decomposition/aging.[61] There was a slight increase in overpotential from 0.02 V (Fig. 2d) to 0.1 V (Fig. 2e) at 0 hour to around 1000 hours. The increased overpotential was contributed by the buildup of the stable solid electrolyte interface (SEI) layer. Impressively, from 1000 hours to 3000 hours (Fig. 2f), the coin cells function smoothly without any rise in overpotential. The stripping/plating of Na using the GPE membrane with different compositions of organic liquid electrolytes (Fig. S2†) shows that GPE41 had the smallest overpotential compared to GPEPC and GPE11. This result reveals that a higher amount of PC is more compatibility with the battery system. The partial dehydrofluorination process of the PVDF backbone results in the formation of a stable Na–F SEI, as reported in a previous study.[62,63] The rich Na–F SEI layer not only stabilizes the sodium ion deposition, but also restrains the growth of dendrite effectively.[62,64–68] These contributions enable excellent cycling performance in Na|GPE41|Na for 3000 hours progression. A plating and stripping test with alternatetive current density rate was conducted for Na|GPE41|Na coin cells, shown in Fig. S3.† The result indicates that GPE41 can steadily operate from 0.1 to 0.4 mA cm^2 and only failed at 0.5 mA cm^2 current density. The PVDF-based GPE membrane shows an excellent suppression toward the dendrite formation at the electrodes' surface and an effective interfacial contact between the electrode and electrolyte. As a result, the coin cell was able to run for extremely long period without any short-circuit. Moreover, our result proves that the GPE membrane can function as both the separator and the ion transport medium with rigid mechanical strength and can tolerate high expansion and contraction of sodium electrode during charge and discharge. The membrane can be utilized for not only sodium sulfur batteries but also sodium ion energy storage.

The transference number of Na^+ (t_{Na^+}) is a parameter describing Na^+ migration, which is crucial in NaSBs. The value of t_{Na} was evaluated using combined AC and DC polarization techniques shown in Fig. 3.[69,70] In this technique, the GPE was polarized by applying a small constant voltage of 10 mV across the Na|GPE|Na coin cell for 5 hours. Bulk resistances of the cell were measured using electrochemical impedance spectroscopy (EIS) before and after the polarization process. The t_{Na^+} of GPE41 was calculated to be 0.648 using the following equation:

$$t_{Na^+} = \frac{I_s(\Delta V - R_o I_o)}{I_o(\Delta V - R_s I_s)} \quad (3)$$

where R_o, R_s, I_o, I_s and ΔV are the initial resistance, steady-state resistance, initial current, steady-state current and polar-

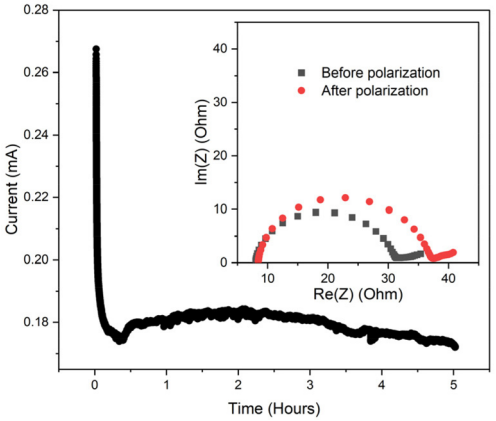

Fig. 3 Polarization of Na|GPE41|Na with the inset of EIS before and after polarization.

ized voltage, respectively. t_{Na^+} in this work is found to be significantly higher than previous studies 0.37[51] and 0.49[52] .[71–73] In conventional sodium-based electrolytes, because the solvation of Na^+ with the solvent is stronger than the solvation of anions, the solvent t_{Na^+} is typically less than 0.5.[74] A higher sodium-ion transport is crucial in NaSBs. This means that a larger fraction of the total current is carried by sodium ions, resulting in minimizing the concentration polarization.

The oxidation and reduction potential as well as the reversibility and electrolyte stability of full-cell Na|GPE41|SPAN were conducted *via* cyclic voltammetry (CV), shown in Fig. 4a.[75] Additionally, the CV curves provide insights into the reaction kinetics based on the voltage applied and the corresponding current. The CV curves displayed in Fig. 4a reveal the major differences during the redox reaction process at the working electrode surface. During the initial cathodic scan, the current slope starts at around 1.5 V *vs.* Na/Na^+, corresponding to the solid–liquid transition from sulfur to dissolved Na_2S_x (x = 4–8), and the peak at 1 V is related to the formation of solid Na_2S

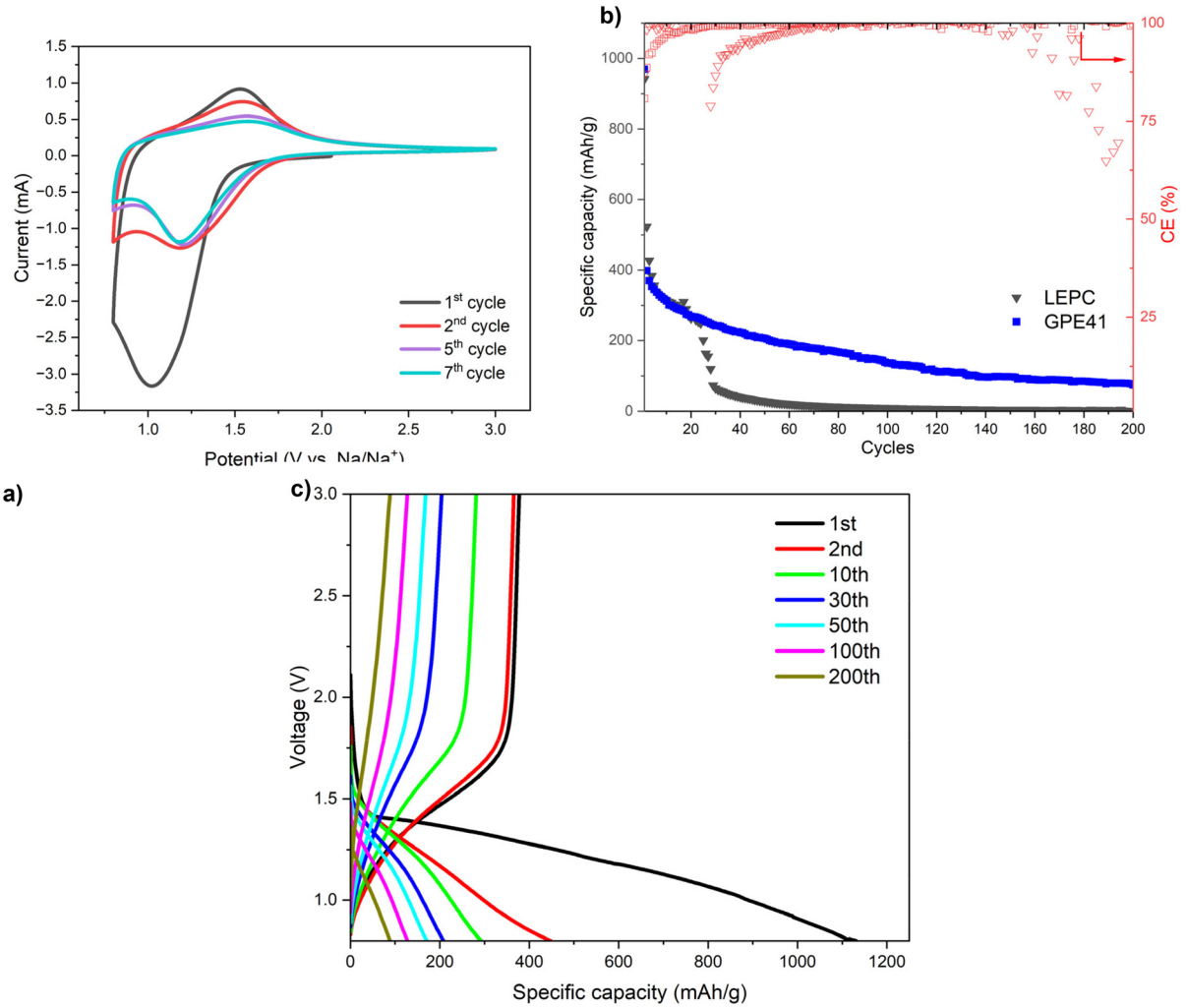

Fig. 4 (a) Cyclic voltammetry of Na|GPE41|SPAN with 0.1 mV s^{-1} scan rate and 0.8 V–3 V potential window. (b) Capacity *versus* cycle from the galvanostatic charge and discharge test of full-cell Na|GPE41|SPAN at 0.1C. (c) Voltage profiles of full-cell Na|GPE41|SPAN long cycle at 0.1C.

and Na_2S_2, as observed during the first cycle.[49,76] The irreversible peak is characteristic of the SPAN cathode.[31] In a subsequent cycle, this discharge peak shifted to 1.2 V. The peak shifts during the second cycle go along with a considerable reduction in the polarization of the electrodes during cycling. During discharge, both of the peaks indicate the formation of Na_2S_2 and Na_2S.[77] Upon charging, Na_2S is converted into polysulfides (S_x) at around 1.7 V and all sulfur is bound to PAN in the fully charged state above 2.28 V *vs.* Na/Na^+.[78,79] After the 2nd cycle, the repetition of CV redox peaks (Fig. 4a) 2nd–7th cycle confirms that the GPE41 membrane acts as a functional separator, which facilitated the Na-SPAN cells to run multiple cycles.

Long-term galvanostatic cycling of two Na-SPAN cells incorporating GPE41 and LEPC was conducted for 200 cycles (Fig. 4b). The battery test illustrates the stability of the cells and the high reversibility at 0.1 C. GCD shows that the GPE41 cell exhibited an initial specific capacity of ~1000 mA h g^{-1} with a reversible capacity of ~398 mA h g^{-1}. With the longevity examination, the LEPC cell failed after 25 cycles, whereas GPE still ran steadily to 200 cycles with 99% Coulomb efficiency (CE) and maintained a specific capacity of 74 mA h g^{-1}. With the help of the rich Na–F SEI layer from dehydrofluorination of the PVDF-HFP polymer and the incorporation of GPE membrane prevented the short circuit happening in the cells.[42,66,67,80] This synergistic effect allows the batteries to run an extensive cycle compared to the conventional LE batteries. The results further support the sodium ion uniform deposition using the GPE in both full-cell and half-cell configurations. The comparison of full cells using GPEPC, GPE11 and GPE41 is shown in Fig. S4† where all of the cells were able to maintain long cycles without any short circuit with ~99% CE. Of all, GPE41 provides better compatibility between the electrode and the electrolyte and was capable of discharging higher 1st and 2nd specific capacities of 1125 and 458 mA h g_{sulfur}^{-1} than the other cells. Fig. 4c shows the voltage profile of the GPE cell at different cycles. The voltage profile has a consistent charging plateau of around 1.6 V which is in agreement with CV results (Fig. 4a). The voltage profiles do not show any shape change or any additional plateau, indicating that the GPE matrix does not decompose or have any side reaction after a long cycling time.

5. Conclusion

We have successfully prepared a PVDF-HFP-based GPE incorporating $NaClO_4$ and organic electrolytes with different ratios *via* a solution casting technique. Galvanostatic plating and stripping performed using a Na|GPE41|Na cell exhibit a long-stability lifespan up to 3000 hours of operation without any GPE41 membrane, which can achieve a high ionic conductivity of 1.37 mS cm^{-1}, high t_{Na^+} of ~0.648 at room temperature and an electrochemical stability window of 4.5 V *vs.* Na^+/Na. Na-SPAN cells employed a GPE41 electrolyte and delivered a discharge capacity of 398 mA h g_{sulfur}^{-1} at the 1st reversible cycle and 75 mA h g_{sulfur}^{-1} after cycling for 200 cycles with 99% CE. The incorporation of GPEs in Na-SPAN batteries at ambient temperatures presents a promising avenue for advancing sodium–sulfur batteries technology. By utilizing GPEs, we anticipate a new paradigm in sodium–sulfur battery development, addressing key challenges and opening up innovative possibilities for high-performance, safer energy storage solutions.

Abbreviations

LEs	Liquid electrolytes
PEs	Polymer electrolytes
GPEs	Gel polymer electrolytes
LEPC	1 M $NaClO_4$ in PC
LE11	1 M $NaClO_4$ in PC : EC (1 : 1 v/v)
LE41	1 M $NaClO_4$ in PC : EC (4 : 1 v/v)
GPEPC	GPE has LEPC entrapped in PVDF-HFP after vacuum drying and swell after immersing LEPC
GPE11	GPE has LE11 entrapped in PVDF-HFP after vacuum drying and swell after immersing LE11
GPE41	GPE has LE41 entrapped in PVDF-HFP after vacuum drying and swell after immersing in LE41

Data availability

The data generated and/or analyzed during the current study are available from the corresponding author upon reasonable request. The supplementary data that support the findings of this study are openly available.

Conflicts of interest

There are no conflicts to declare.

Acknowledgements

This work was supported by the National Science Foundation under Award 2229305.

References

1 B. Dunn, H. Kamath and J.-M. Tarascon, Electrical Energy Storage for the Grid: A Battery of Choices, *Science*, 2011, **334**(6058), 928–935, DOI: 10.1126/science.1212741.
2 L. Gaines, The Future of Automotive Lithium-Ion Battery Recycling: Charting a Sustainable Course, *Sustainable Mater. Technol.*, 2014, **1–2**, 2–7, DOI: 10.1016/j.susmat.2014.10.001.
3 M. Pigłowska, B. Kurc, M. Galiński, P. Fuć, M. Kamińska, N. Szymlet and P. Daszkiewicz, Challenges for Safe

Electrolytes Applied in Lithium-Ion Cells—A Review, *Materials*, 2021, **14**(22), 6783, DOI: 10.3390/ma14226783.
4 Q. Wang, L. Jiang, Y. Yu and J. Sun, Progress of Enhancing the Safety of Lithium Ion Battery from the Electrolyte Aspect, *Nano Energy*, 2019, **55**, 93–114, DOI: 10.1016/j.nanoen.2018.10.035.
5 K. Liu, Y. Liu, D. Lin, A. Pei and Y. Cui, Materials for Lithium-Ion Battery Safety, *Sci. Adv.*, 2018, **4**(6), eaas9820, DOI: 10.1126/sciadv.aas9820.
6 Y. Zhu, Y. Yang, L. Fu and Y. Wu, A Porous Gel-Type Composite Membrane Reinforced by Nonwoven: Promising Polymer Electrolyte with High Performance for Sodium Ion Batteries, *Electrochim. Acta*, 2017, **224**, 405–411, DOI: 10.1016/j.electacta.2016.12.030.
7 K. Vignarooban, R. Kushagra, A. Elango, P. Badami, B.-E. Mellander, X. Xu, T. G. Tucker, C. Nam and A. M. Kannan, Current Trends and Future Challenges of Electrolytes for Sodium-Ion Batteries, *Int. J. Hydrogen Energy*, 2016, **41**(4), 2829–2846, DOI: 10.1016/j.ijhydene.2015.12.090.
8 D.-W. Kang and J.-K. Kim, Characterization of Fibrous Gel Polymer Electrolyte for Lithium Polymer Batteries with Enhanced Electrochemical Properties, *J. Electroanal. Chem.*, 2016, **775**, 37–42, DOI: 10.1016/j.jelechem.2016.05.029.
9 D. Kumar, M. Suleman and S. A. Hashmi, Studies on Poly (Vinylidene Fluoride-Co-Hexafluoropropylene) Based Gel Electrolyte Nanocomposite for Sodium–Sulfur Batteries, *Solid State Ionics*, 2011, **202**(1), 45–53, DOI: 10.1016/j.ssi.2011.09.001.
10 M. J. Park, I. Choi, J. Hong and O. Kim, Polymer Electrolytes Integrated with Ionic Liquids for Future Electrochemical Devices, *J. Appl. Polym. Sci.*, 2013, **129**(5), 2363–2376, DOI: 10.1002/app.39064.
11 J. Kalhoff, G. G. Eshetu, D. Bresser and S. Passerini, Safer Electrolytes for Lithium-Ion Batteries: State of the Art and Perspectives, *ChemSusChem*, 2015, **8**(13), 2154–2175, DOI: 10.1002/cssc.201500284.
12 I. Osada, H. de Vries, B. Scrosati and S. Passerini, Ionic-Liquid-Based Polymer Electrolytes for Battery Applications, *Angew. Chem., Int. Ed.*, 2016, **55**(2), 500–513, DOI: 10.1002/anie.201504971.
13 S. Tan, Y. J. Ji, Z. R. Zhang and Y. Yang, Recent Progress in Research on High-Voltage Electrolytes for Lithium-Ion Batteries, *ChemPhysChem*, 2014, **15**(10), 1956–1969, DOI: 10.1002/cphc.201402175.
14 J. I. Kim, Y. Choi, K. Y. Chung and J. H. Park, A Structurable Gel-Polymer Electrolyte for Sodium Ion Batteries, *Adv. Funct. Mater.*, 2017, **27**(34), 1701768, DOI: 10.1002/adfm.201701768.
15 Y. Zhu, S. Xiao, Y. Shi, Y. Yang, Y. Hou and Y. Wu, A Composite Gel Polymer Electrolyte with High Performance Based on Poly(Vinylidene Fluoride) and Polyborate for Lithium Ion Batteries, *Adv. Energy Mater.*, 2014, **4**(1), 1300647, DOI: 10.1002/aenm.201300647.
16 Y. Q. Yang, Z. Chang, M. X. Li, X. W. Wang and Y. P. Wu, A Sodium Ion Conducting Gel Polymer Electrolyte, *Solid State Ionics*, 2015, **269**, 1–7, DOI: 10.1016/j.ssi.2014.11.015.
17 J. Nunes-Pereira, C. M. Costa and S. Lanceros-Méndez, Polymer Composites and Blends for Battery Separators: State of the Art, Challenges and Future Trends, *J. Power Sources*, 2015, **281**, 378–398, DOI: 10.1016/j.jpowsour.2015.02.010.
18 X. Cheng, J. Pan, Y. Zhao, M. Liao and H. Peng, Gel Polymer Electrolytes for Electrochemical Energy Storage, *Adv. Energy Mater.*, 2018, **8**(7), 1702184, DOI: 10.1002/aenm.201702184.
19 J. Muldoon, C. B. Bucur, N. Boaretto, T. Gregory and V. di Noto, Polymers: Opening Doors to Future Batteries, *Polym. Rev.*, 2015, **55**(2), 208–246, DOI: 10.1080/15583724.2015.1011966.
20 H. Nguyen and S. Wei, Recent Progress of Gel Polymer Electrolytes for Sodium Sulfur Batteries, *ACS Appl. Electron. Mater.*, 2024, **6**(12), 8671–8688, DOI: 10.1021/acsaelm.3c01841.
21 M. B. Armand, Polymer Electrolytes, *Annu. Rev. Mater. Sci.*, 1986, **16**(1), 245–261, DOI: 10.1146/annurev.ms.16.080186.001333.
22 A. Arya and A. L. Sharma, Polymer Electrolytes for Lithium Ion Batteries: A Critical Study, *Ionics*, 2017, **23**(3), 497–540, DOI: 10.1007/s11581-016-1908-6.
23 D. Zhou, D. Shanmukaraj, A. Tkacheva, M. Armand and G. Wang, Polymer Electrolytes for Lithium-Based Batteries: Advances and Prospects, *Chem*, 2019, **5**(9), 2326–2352, DOI: 10.1016/j.chempr.2019.05.009.
24 S. Abbrent, J. Plestil, D. Hlavata, J. Lindgren, J. Tegenfeldt and Å. Wendsjö, Crystallinity and Morphology of PVdF–HFP-Based Gel Electrolytes, *Polymer*, 2001, **42**(4), 1407–1416, DOI: 10.1016/S0032-3861(00)00517-6.
25 S. Janakiraman, O. Padmaraj, S. Ghosh and A. Venimadhav, A Porous Poly (Vinylidene Fluoride-Co-Hexafluoropropylene) Based Separator-Cum-Gel Polymer Electrolyte for Sodium-Ion Battery, *J. Electroanal. Chem.*, 2018, **826**, 142–149, DOI: 10.1016/j.jelechem.2018.08.032.
26 T. Liu, Z. Chang, Y. Yin, K. Chen, Y. Zhang and X. Zhang, The PVDF-HFP Gel Polymer Electrolyte for Li-O2 Battery, *Solid State Ionics*, 2018, **318**, 88–94, DOI: 10.1016/j.ssi.2017.08.001.
27 C. Ribeiro, C. M. Costa, D. M. Correia, J. Nunes-Pereira, J. Oliveira, P. Martins, R. Gonçalves, V. F. Cardoso and S. Lanceros-Méndez, Electroactive Poly(Vinylidene Fluoride)-Based Structures for Advanced Applications, *Nat. Protoc.*, 2018, **13**(4), 681–704, DOI: 10.1038/nprot.2017.157.
28 S. H. Senthilkumar, B. Ramasubramanian, R. P. Rao, V. Chellappan and S. Ramakrishna, Advances in Electrospun Materials and Methods for Li-Ion Batteries, *Polymers*, 2023, **15**(7), 1622, DOI: 10.3390/polym15071622.
29 J. C. Barbosa, J. P. Dias, S. Lanceros-Méndez and C. M. Costa, Recent Advances in Poly(Vinylidene Fluoride) and Its Copolymers for Lithium-Ion Battery Separators, *Membranes*, 2018, **8**(3), 45, DOI: 10.3390/membranes8030045.
30 L. Zhou, Q. Cao, B. Jing, X. Wang, X. Tang and N. Wu, Study of a Novel Porous Gel Polymer Electrolyte Based on

Thermoplastic Polyurethane/Poly(Vinylidene Fluoride-Co-Hexafluoropropylene) by Electrospinning Technique, *J. Power Sources*, 2014, **263**, 118–124, DOI: 10.1016/j.jpowsour.2014.03.140.

31 S. Wei, L. Ma, K. E. Hendrickson, Z. Tu and L. A. Archer, Metal–Sulfur Battery Cathodes Based on PAN–Sulfur Composites, *J. Am. Chem. Soc.*, 2015, **137**(37), 12143–12152, DOI: 10.1021/jacs.5b08113.

32 G. P. Pandey and S. A. Hashmi, Experimental Investigations of an Ionic-Liquid-Based, Magnesium Ion Conducting, Polymer Gel Electrolyte, *J. Power Sources*, 2009, **187**(2), 627–634, DOI: 10.1016/j.jpowsour.2008.10.112.

33 D. Kumar and S. A. Hashmi, Ionic Liquid Based Sodium Ion Conducting Gel Polymer Electrolytes, *Solid State Ionics*, 2010, **181**(8), 416–423, DOI: 10.1016/j.ssi.2010.01.025.

34 V. Aravindan and P. Vickraman, Lithium Fluoroalkylphosphate Based Novel Composite Polymer Electrolytes (NCPE) Incorporated with Nanosized SiO_2 Filler, *Mater. Chem. Phys.*, 2009, **115**(1), 251–257, DOI: 10.1016/j.matchemphys.2008.11.062.

35 D. Saikia, H.-Y. Wu, Y.-C. Pan, C.-P. Lin, K.-P. Huang, K.-N. Chen, G. T. K. Fey and H.-M. Kao, Highly Conductive and Electrochemically Stable Plasticized Blend Polymer Electrolytes Based on PVdF-HFP and Triblock Copolymer PPG-PEG-PPG Diamine for Li-Ion Batteries, *J. Power Sources*, 2011, **196**(5), 2826–2834, DOI: 10.1016/j.jpowsour.2010.10.096.

36 Z. Li, G. Su, X. Wang and D. Gao, Micro-Porous P(VDF-HFP)-Based Polymer Electrolyte Filled with Al_2O_3 Nanoparticles, *Solid State Ionics*, 2005, **176**(23), 1903–1908, DOI: 10.1016/j.ssi.2005.05.006.

37 X. Zhang, T. Liu, S. Zhang, X. Huang, B. Xu, Y. Lin, B. Xu, L. Li, C.-W. Nan and Y. Shen, Synergistic Coupling between Li6.75La3Zr1.75Ta0.25O12 and Poly(Vinylidene Fluoride) Induces High Ionic Conductivity, Mechanical Strength, and Thermal Stability of Solid Composite Electrolytes, *J. Am. Chem. Soc.*, 2017, **139**(39), 13779–13785, DOI: 10.1021/jacs.7b06364.

38 Y. Zhao, Y. Bai, Y. Bai, M. An, G. Chen, W. Li, C. Li and Y. Zhou, A Rational Design of Solid Polymer Electrolyte with High Salt Concentration for Lithium Battery, *J. Power Sources*, 2018, **407**, 23–30, DOI: 10.1016/j.jpowsour.2018.10.045.

39 B. Wang, H. P. Zhang, L. C. Yang, Q. T. Qu, Y. P. Wu, C. L. Gan and D. L. Zhou, Improving Electrochemical Performance of Graphitic Carbon in PC-Based Electrolytes by Using *N*-Vinyl-2-Pyrrolidone as an Additive, *Electrochem. Commun.*, 2008, **10**(10), 1571–1574, DOI: 10.1016/j.elecom.2008.08.018.

40 U. R. Farooqui, A. L. Ahmad and N. A. Hamid, Effect of Polyaniline (PANI) on Poly(Vinylidene Fluoride-Co-Hexaflouro Propylene) (PVDF-Co-HFP) Polymer Electrolyte Membrane Prepared by Breath Figure Method, *Polym. Test.*, 2017, **60**, 124–131, DOI: 10.1016/j.polymertesting.2017.03.012.

41 J. Jie, Y. Liu, L. Cong, B. Zhang, W. Lu, X. Zhang, J. Liu, H. Xie and L. Sun, High-Performance PVDF-HFP Based Gel Polymer Electrolyte with a Safe Solvent in Li Metal Polymer Battery, *J. Energy Chem.*, 2020, **49**, 80–88, DOI: 10.1016/j.jechem.2020.01.019.

42 J. Castillo, A. Robles-Fernandez, R. Cid, J. A. González-Marcos, M. Armand, D. Carriazo, H. Zhang and A. Santiago, Dehydrofluorination Process of Poly (Vinylidene Difluoride) PVdF-Based Gel Polymer Electrolytes and Its Effect on Lithium-Sulfur Batteries, *Gels*, 2023, **9**(4), 336, DOI: 10.3390/gels9040336.

43 D. Mouraliraman, N. Shaji, S. Praveen, M. Nanthagopal, C. W. Ho, M. Varun Karthik, T. Kim and C. W. Lee, Thermally Stable PVDF-HFP-Based Gel Polymer Electrolytes for High-Performance Lithium-Ion Batteries, *Nanomaterials*, 2022, **12**(7), 1056, DOI: 10.3390/nano12071056.

44 G. Peng, X. Zhao, Z. Zhan, S. Ci, Q. Wang, Y. Liang and M. Zhao, New Crystal Structure and Discharge Efficiency of Poly(Vinylidene Fluoride-Hexafluoropropylene)/Poly(Methyl Methacrylate) Blend Films, *RSC Adv.*, 2014, **4**(32), 16849–16854, DOI: 10.1039/C3RA47462C.

45 Y. P. Mahant, S. B. Kondawar, D. V. Nandanwar and P. Koinkar, Poly(Methyl Methacrylate) Reinforced Poly (Vinylidene Fluoride) Composites Electrospun Nanofibrous Polymer Electrolytes as Potential Separator for Lithium Ion Batteries, *Mater. Renew. Sustain. energy*, 2018, **7**(2), 5, DOI: 10.1007/s40243-018-0115-y.

46 M. Tanwar, H. K. Bezabh, S. Basu, W.-N. Su and B.-J. Hwang, Investigation of Sodium Plating and Stripping on a Bare Current Collector with Different Electrolytes and Cycling Protocols, *ACS Appl. Mater. Interfaces*, 2019, **11**(43), 39746–39756, DOI: 10.1021/acsami.9b10097.

47 S. Xin, Y.-X. Yin, Y.-G. Guo and L.-J. Wan, A High-Energy Room-Temperature Sodium-Sulfur Battery, *Adv. Mater.*, 2014, **26**(8), 1261–1265, DOI: 10.1002/adma.201304126.

48 S. Wei, S. Xu, A. Agrawral, S. Choudhury, Y. Lu, Z. Tu, L. Ma and L. A. Archer, A Stable Room-Temperature Sodium–Sulfur Battery, *Nat. Commun.*, 2016, **7**(1), 11722, DOI: 10.1038/ncomms11722.

49 S. Murugan, S. Niesen, J. Kappler, K. Küster, U. Starke and M. R. Buchmeiser, Ultra-Stable Cycling of High Capacity Room Temperature Sodium-Sulfur Batteries Based on Sulfurated Poly(Acrylonitrile), *Batteries Supercaps*, 2021, **4**(10), 1636–1646, DOI: 10.1002/batt.202100125.

50 A. Manthiram and X. Yu, Ambient Temperature Sodium–Sulfur Batteries, *Small*, 2015, **11**(18), 2108–2114, DOI: 10.1002/smll.201403257.

51 Y.-X. Wang, B. Zhang, W. Lai, Y. Xu, S.-L. Chou, H.-K. Liu and S.-X. Dou, Room-Temperature Sodium-Sulfur Batteries: A Comprehensive Review on Research Progress and Cell Chemistry, *Adv. Energy Mater.*, 2017, **7**(24), 1602829, DOI: 10.1002/aenm.201602829.

52 C. Zhao, L. Liu, X. Qi, Y. Lu, F. Wu, J. Zhao, Y. Yu, Y.-S. Hu and L. Chen, Solid-State Sodium Batteries, *Adv. Energy Mater.*, 2018, **8**(17), 1703012, DOI: 10.1002/aenm.201703012.

53 X. Liu, X. Jiang, Z. Zeng, X. Ai, H. Yang, F. Zhong, Y. Xia and Y. Cao, High Capacity and Cycle-Stable Hard Carbon

Anode for Nonflammable Sodium-Ion Batteries, *ACS Appl. Mater. Interfaces*, 2018, **10**(44), 38141–38150, DOI: **10.1021/acsami.8b16129**.

54 R. Baskaran, S. Selvasekarapandian, N. Kuwata, J. Kawamura and T. Hattori, Ac Impedance, DSC and FT-IR Investigations on (*x*)PVAc–(1 − *x*)PVdF Blends with LiClO4, *Mater. Chem. Phys.*, 2006, **98**(1), 55–61, DOI: **10.1016/j.matchemphys.2005.08.063**.

55 R. Dallaev, T. Pisarenko, D. Sobola, F. Orudzhev, S. Ramazanov and T. Trčka, Brief Review of PVDF Properties and Applications Potential, *Polymers*, 2022, **14**(22), 4793, DOI: **10.3390/polym14224793**.

56 G. Peng, X. Zhao, Z. Zhan, S. Ci, Q. Wang, Y. Liang and M. Zhao, New Crystal Structure and Discharge Efficiency of Poly(Vinylidene Fluoride-Hexafluoropropylene)/Poly(Methyl Methacrylate) Blend Films, *RSC Adv.*, 2014, **4**(32), 16849–16854, DOI: **10.1039/C3RA47462C**.

57 A. M. Voice, J. P. Southall, V. Rogers, K. H. Matthews, G. R. Davies, J. E. McIntyre and I. M. Ward, Thermoreversible Polymer Gel Electrolytes, *Polymer*, 1994, **35**(16), 3363–3372, DOI: **10.1016/0032-3861(94)90896-6**.

58 C. V. Subba Reddy, A. K. Sharma and V. V. R. Narasimha Rao, Conductivity and Discharge Characteristics of Polyblend (PVP+PVA+KIO3) Electrolyte, *J. Power Sources*, 2003, **114**(2), 338–345, DOI: **10.1016/S0378-7753(02)00582-7**.

59 Z. Deng, T. P. Mishra, E. Mahayoni, Q. Ma, A. J. K. Tieu, O. Guillon, J.-N. Chotard, V. Seznec, A. K. Cheetham, C. Masquelier, G. S. Gautam and P. Canepa, Fundamental Investigations on the Sodium-Ion Transport Properties of Mixed Polyanion Solid-State Battery Electrolytes, *Nat. Commun.*, 2022, **13**(1), 4470, DOI: **10.1038/s41467-022-32190-7**.

60 A. V. Karatrantos, S. Khan, C. Yan, R. Dieden, K. Urita, T. Ohba and Q. Cai, Ion Transport in Organic Electrolyte Solutions for Lithium-Ion Batteries and Beyond, *J. Energy Power Technol.*, 2021, **3**(3), 1–36, DOI: **10.21926/jept.2103043**.

61 C. Fang, T.-N. Tran, Y. Zhao and G. Liu, Electrolyte Decomposition and Solid Electrolyte Interphase Revealed by Mass Spectrometry, *Electrochim. Acta*, 2021, **399**, 139362, DOI: **10.1016/j.electacta.2021.139362**.

62 M. A. Muñoz-Márquez, M. Zarrabeitia, E. Castillo-Martínez, A. Eguía-Barrio, T. Rojo and M. Casas-Cabanas, Composition and Evolution of the Solid-Electrolyte Interphase in Na2Ti3O7 Electrodes for Na-Ion Batteries: XPS and Auger Parameter Analysis, *ACS Appl. Mater. Interfaces*, 2015, **7**(14), 7801–7808, DOI: **10.1021/acsami.5b01375**.

63 X. Zhang, S. Wang, C. Xue, C. Xin, Y. Lin, Y. Shen, L. Li and C.-W. Nan, Self-Suppression of Lithium Dendrite in All-Solid-State Lithium Metal Batteries with Poly(Vinylidene Difluoride)-Based Solid Electrolytes, *Adv. Mater.*, 2019, **31**(11), 1806082, DOI: **10.1002/adma.201806082**.

64 J. Chen, T. Liu, M. Chu, K. Yu, X. Xie, K. Lin, Y. Cheng, X. Zhang, J. Li and Z. Shi, Insight into the Interfacial Reaction Mechanism of FEC and NaF on Na for High Performance Sodium Metal Batteries., *J. Mater. Chem. A*, 2024, **12**(37), 25222–25232, DOI: **10.1039/D4TA03266G**.

65 M.Á Muñoz-Márquez, M. Zarrabeitia, S. Passerini and T. Rojo, Structure, Composition, Transport Properties, and Electrochemical Performance of the Electrode-Electrolyte Interphase in Non-Aqueous Na-Ion Batteries, *Adv. Mater. Interfaces*, 2022, **9**(8), 2101773, DOI: **10.1002/admi.202101773**.

66 M. Xu, Y. Li, M. Ihsan-Ul-Haq, N. Mubarak, Z. Liu, J. Wu, Z. Luo and J. K. Kim, NaF-Rich Solid Electrolyte Interphase for Dendrite-Free Sodium Metal Batteries, *Energy Storage Mater.*, 2022, **44**, 477–486, DOI: **10.1016/j.ensm.2021.10.038**.

67 C. Zhu, D. Wu, Z. Wang, H. Wang, J. Liu, K. Guo, Q. Liu and J. Ma, Optimizing NaF-Rich Solid Electrolyte Interphase for Stabilizing Sodium Metal Batteries by Electrolyte Additive, *Adv. Funct. Mater.*, 2024, **34**(5), 2214195, DOI: **10.1002/adfm.202214195**.

68 K. Kubota and S. Komaba, Review—Practical Issues and Future Perspective for Na-Ion Batteries, *J. Electrochem. Soc.*, 2015, **162**(14), A2538, DOI: **10.1149/2.0151514jes**.

69 J. B. Wagner and C. Wagner, Electrical Conductivity Measurements on Cuprous Halides, *J. Chem. Phys.*, 1957, **26**(6), 1597–1601, DOI: **10.1063/1.1743590**.

70 J. Evans, C. A. Vincent and P. G. Bruce, Electrochemical Measurement of Transference Numbers in Polymer Electrolytes, *Polymer*, 1987, **28**(13), 2324–2328, DOI: **10.1016/0032-3861(87)90394-6**.

71 D. Lei, Y.-B. He, H. Huang, Y. Yuan, G. Zhong, Q. Zhao, X. Hao, D. Zhang, C. Lai, S. Zhang, J. Ma, Y. Wei, Q. Yu, W. Lv, Y. Yu, B. Li, Q.-H. Yang, Y. Yang, J. Lu and F. Kang, Cross-Linked Beta Alumina Nanowires with Compact Gel Polymer Electrolyte Coating for Ultra-Stable Sodium Metal Battery, *Nat. Commun.*, 2019, **10**(1), 4244, DOI: **10.1038/s41467-019-11960-w**.

72 Y. Lu, L. Li, Q. Zhang, Y. Cai, Y. Ni and J. Chen, High-Performance All-Solid-State Electrolyte for Sodium Batteries Enabled by the Interaction between the Anion in Salt and Na 3 SbS 4, *Chem. Sci.*, 2022, **13**(12), 3416–3423, DOI: **10.1039/D1SC06745A**.

73 Q. Ma, J. Liu, X. Qi, X. Rong, Y. Shao, W. Feng, J. Nie, Y.-S. Hu, H. Li, X. Huang, L. Chen and Z. Zhou, A New Na [(FSO2)(n-C4F9SO2)N]-Based Polymer Electrolyte for Solid-State Sodium Batteries, *J. Mater. Chem. A*, 2017, **5**(17), 7738–7743, DOI: **10.1039/C7TA01820G**.

74 F. Huang, P. Xu, G. Fang and S. Liang, In-Depth Understanding of Interfacial Na+ Behaviors in Sodium Metal Anode: Migration, Desolvation, and Deposition, *Adv. Mater.*, 2024, **36**(41), 2405310, DOI: **10.1002/adma.202405310**.

75 X. Huang, Z. Wang, R. Knibbe, B. Luo, S. A. Ahad, D. Sun and L. Wang, Cyclic Voltammetry in Lithium–Sulfur Batteries—Challenges and Opportunities, *Energy Technol.*, 2019, **7**(8), 1801001, DOI: **10.1002/ente.201801001**.

76 X. Xu, D. Zhou, X. Qin, K. Lin, F. Kang, B. Li, D. Shanmukaraj, T. Rojo, M. Armand and G. Wang, A Room-Temperature Sodium–Sulfur Battery with High

Capacity and Stable Cycling Performance, *Nat. Commun.*, 2018, **9**(1), 3870, DOI: **10.1038/s41467-018-06443-3**.

77 S. Ma, P. Zuo, H. Zhang, Z. Yu, C. Cui, M. He and G. Yin, Iodine-Doped Sulfurized Polyacrylonitrile with Enhanced Electrochemical Performance for Room-Temperature Sodium/Potassium Sulfur Batteries, *Chem. Commun.*, 2019, **55**(36), 5267–5270, DOI: **10.1039/C9CC01612K**.

78 A. Y. Sheng Eng, D.-T. Nguyen, V. Kumar, G. Sandhya Subramanian, M.-F. Ng and Z. Wei Seh, Tailoring Binder–Cathode Interactions for Long-Life Room-Temperature Sodium–Sulfur Batteries, *J. Mater. Chem. A*, 2020, **8**(43), 22983–22997, DOI: **10.1039/D0TA07681C**.

79 S. S. Zhang, Understanding of Sulfurized Polyacrylonitrile for Superior Performance Lithium/Sulfur Battery, *Energies*, 2014, **7**(7), 4588–4600, DOI: **10.3390/en7074588**.

80 P. Zhang, R. Li, J. Huang, B. Liu, M. Zhou, B. Wen, Y. Xia and S. Okada, Flexible Poly(Vinylidene Fluoride-Co-Hexafluoropropylene)-Based Gel Polymer Electrolyte for High-Performance Lithium-Ion Batteries, *RSC Adv.*, 2021, **11**(20), 11943–11951, DOI: **10.1039/D1RA01250A**.